Bachelor's Thesis

Testmessung mit Modulen für den ATLAS ITk Pixel Detektor

Test with Modules for the ATLAS ITk Pixel Detector

prepared by

Niklas Grün

from Zeven

at the II. Physikalischen Institut

Zusammenfassung

Derzeit laufen die Vorbereitungen des Upgrades des Large Hadron Colliders (Lhc) zum High Luminosity-Lhc (HL-Lhc). Um das Atlas Experiment auf die steigende Anzahl an Kollisionen vorzubereiten, wird der Inner Detector (ID) durch einen vollständig aus Silizium-Halbleiterdetektoren bestehenden Inner Tracker (ITk), ersetzt. Gegenwärtig befindet sich das ITk Projekt in der Vorproduktionsphase. Ein Teil der Module des Pixeldetektors wird am II. Physikalischen Institut in Göttingen gebaut und getestet. Der HL-Lhc wird wissenschaftlichen Fortschritt bringen unter der Voraussetzung, dass der neue Pixel Detektor unter extremsten Bedingungen funktioniert. Um einen zuverlässigen Betrieb des ITk Pixel Detektors zu gewährleisten, ist es wichtig, die Module vorher zu testen. Ein ausschlaggebender Aspekt sind dabei die elektrischen Tests, die die operationelle Qualität der Module sichern.

Diese Arbeit zielt darauf ab, das Verhalten der Module des Pixel Detektors zu untersuchen, um seinen Einsatz im HL-Lhc zu verifizieren.

Stichwörter: Teilchenphysik, HL-Lhc, Pixel Detektor, Atlas Experiment, ITk

Abstract

Currently, the preparation for the upgrade of the High Luminosity Large Hadron Collider (HL-Lhc) is ongoing. To prepare the Atlas experiment for the intensified amount of collisions, the Inner Detector (ID) will be replaced by an all-silicon semiconductor detector, the Inner Tracker (ITk). Presently, the ITk project is in preproduction phase. Part of the modules for the Pixel Detector are assembled and tested in the II. Institute of Physics in Göttingen. The HL-Lhc will bring scientific advancement demanding the new Pixel Detector to operate in extreme conditions. To secure the reliable operation of the ITk Pixel Detector, it is essential to test the modules beforehand. A pivotal aspect is electrical tests which secure the operational quality of the modules.

This thesis aims at the investigatoin of the behaviour of the modules for the Pixel Detector with the objective of certifying its service in HL-Lhc.

Keywords: Particle Physics, HL-Lhc, Pixel Detector, Atlas experiment, ITk

Contents

Contents

1 Introduction

The majority of the research done at the CERN Nuclear Research Centre aims of acquiring scientific fundamentals about the Standard Model (SM), the currently most successful theory to describe particles and their interactions. In order to test the SM, the Large Hadron Collider (LHC), the biggest and most powerful particle accelerator ever, accelerates protons or heavy Ions up to very high energies. At nearly the speed of light, bunches of particles are brought to collision. The resulting fragments and new particles are detected and tracked in ingenious experimental setups featuring different kinds of detectors, for example, the ATLAS experiment, further treated in Chapter 4.2. As shown in the schedule (Fig. 1.1), CERN plans to take the first data with the upgraded LHC with higher luminosity, the High-Luminosity Large Hadron Collider (HL-LHC) from 2029. With the HL-LHC, the experiments at CERN face new challenges. ATLAS expects a peak instantaneous luminosity of $7.5 \cdot 10^{34}\,\mathrm{cm^{-2}s^{-1}}$ which is 5 times higher than the current instantaneous luminosity indicating more radiation damage in the detector and higher pileup. The increase in luminosity will benefit the statistical uncertainty of measurements. On top of that, more frequent observations of rare phenomena are predicted. To prepare for the upcoming intensified amount of radiation, the Inner Detector of the ATLAS experiment is upgraded to an all-silicon Inner Tracker (ITk). As a result of the intensified radiation, it is necessary to increase the radiation hardness. The ITk project is currently in pre-production phase. The ITk contains hybrid modules. These modules are sensors, bump bonded with frontend (FE) readout electronics. To ensure reliable and durable functionality under such extreme conditions of operation as near the beamline, the modules are tested, which is part of this work.

The goal of this thesis is to investigate the electrical behaviour of modules for the ITk Pixel Detector. For this, firstly the theoretical background and the context of the ITk project are presented. Next, the assembly procedure of the modules that are subject to this thesis as well as the setup for the electrical tests is described. Afterwards, the different electrical tests are explained. Finally, their results are shown and discussed, before a conclusion and outlook are given.
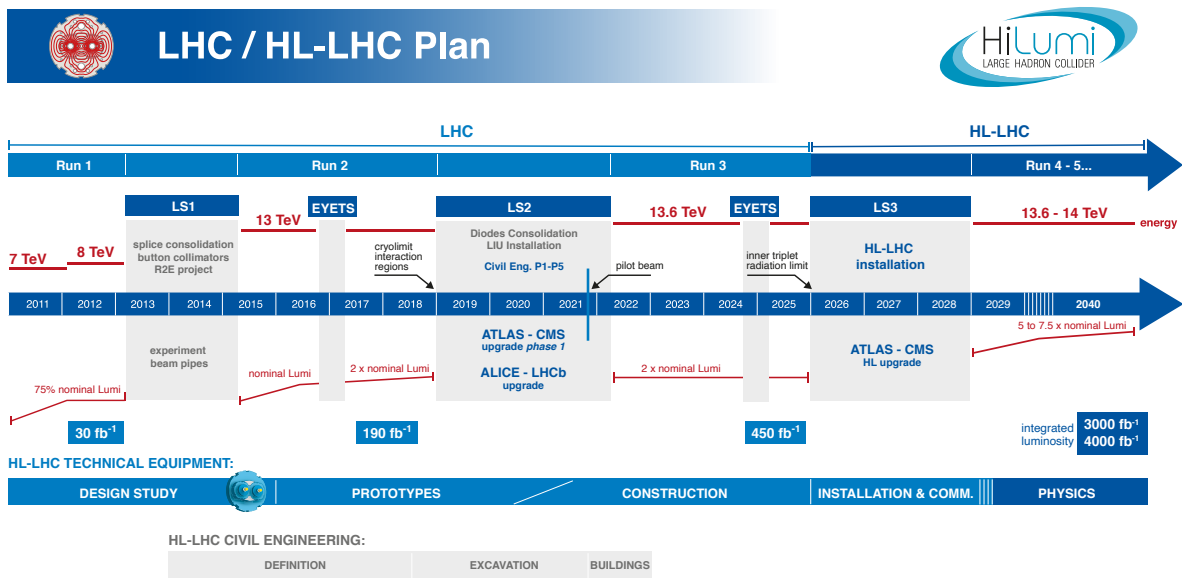
Figure 1.1: Longterm schedule for the operation of Lhc/ HL-Lhc ©Cern.

2 The Standard Model

Containing 17 elementary particles, the Standard Model (SM) of Particle Physics encompasses the current theoretical knowledge base to describe three of the four fundamental forces as interactions between the elementary particles. The Standard Model is a quantum field theory describing all interactions based on a Lagrangian [2–14]. Among the 17 elementary particles, there are 12 with spin $\frac{1}{2}$, the fermions, and 5 that have integer spin, the bosons. There are three generations of fermions with increasing mass per generation. The fermions can be separated into leptons and quarks. There are 6 quarks, equally distributed over the three generations. One quark per generation has an electric charge $+\frac{2}{3}$ (up-type) and the other one electric charge $-\frac{1}{3}$, the down-type quarks [15, 16]. Together they form weak isospin doublets. Just like the quarks, the leptons also form three generations. They are also arranged in isospin doublets, one doublet per generation. A single doublet features an uncharged neutrino with its weak isospin component $+\frac{1}{2}$ and a charged lepton and its weak isospin component $-\frac{1}{2}$. The charged leptons' masses increase with the generations, and the neutrinos are nearly massless.

Among the bosons, there are four mediators of fundamental forces with spin 1, the gauge bosons, and the Higgs boson with spin 0, the latest addition to the Standard Model [17–22]. The gluon carries a colour charge mediating the strong force described by quantum chromodynamics (QCD) [15, 16]. The massless photon is the gauge boson for the electromagnetic force carrying no electric charge [23–30]. The charged $W^{\pm}$ and the neutral Z boson mediate the weak force [4–6]. Figure 2.1 summarises the SM.
On top of that, all particles with an additive quantum number $\neq 0$ have a corresponding antiparticle with the same properties except for the reversed sign on all additive quantum numbers such as electric charge. As a consequence, there are particles that are their own antiparticles, for example, the Higgs boson.

The SM is considered a strong theory unifying three of the four fundamental forces. Nonetheless, it does not yet predict gravity or dark matter, letting us hope for new physics to be discovered for example at the Lhc at Cern.
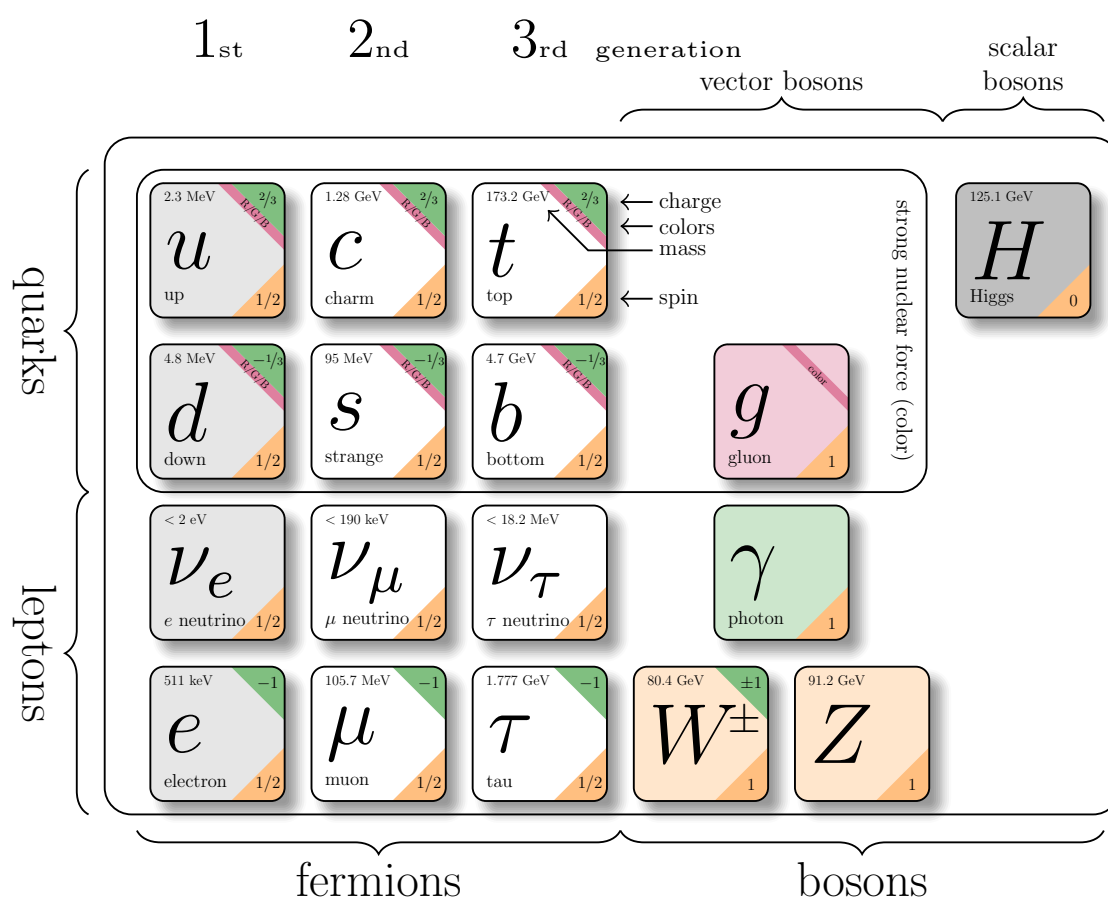
Figure 2.1: Overview of the SM. The data are from Particle Data Group [1].

3 Detectors

3.1 Introduction

Detectors are apparati to count, track, and identify particles. The detection results from a particle's interaction with the detector material. The interaction between particles and material varies between different particles and materials. There are three main interaction processes between a particle and the detector that determine the measuring process:

1. Ionisation and Excitation happen when an incoming particle transfers (part of) its energy to an electron, most likely of an outer shell electron, of the detector material's atoms such that it gains enough energy to escape the binding atomic potential. The remaining Ion is charged, as a neutral atom loses a charge-carrying particle.

2. Bremsstrahlung is electromagnetic radiation emitted when charge-carrying particles are decelerated due to deflection by a charge carrier, in most cases an electron by an atomic nucleus.

3. Photoelectric effect describes the emission of electrons when a material is hit by electromagnetic radiation above a certain energy. This is when the photon has an energy above the binding energy of the electron to the nucleus.

3.2 Bethe-Bloch Formula

The Bethe-Bloch formula shown in Equation (3.1), found by physicists Bethe and Bloch in 1932, describes the mean deposited energy per unit length of a charged particle passing through a material [31, 32]. As one can see in Equation (3.1), the deposited energy depends on the particle type, its charge z (in units of electron charge), and the material properties such as density and atomic number Z

$$-\left\langle \frac{\mathrm{dE}}{\mathrm{dx}} \right\rangle = \frac{4\pi n z^2}{m_e c^2 \beta^2} \cdot \left(\frac{e^2}{4\pi \epsilon_0} \right)^2 \cdot \left[\ln \left(\frac{2m_e c^2 \beta^2}{I(1-\beta^2)} \right) - \beta^2 \right], \qquad (3.1)$$

where $\beta = \frac{v}{c}$, $n = \frac{N_A \cdot Z \cdot \rho}{M_u \cdot A}$ is the electron density, and I is the mean excitation energy, which can be approximated to $I = 10\,\mathrm{eV} \cdot Z$ [32].

As detectors track and identify particles via their interaction with the material, the Bethe-Bloch formula describes the particle-material interaction and therefore the detection process.

There are different types of detectors, e.g. gaseous detectors, calorimeters, and semi-conductor detectors. All of them have specific properties and they vary in size, use, resolution, cost, etc.

Modern large-scale particle physics experiments, such as ATLAS, mostly consist of multiple layers of different detectors (see Section 4.2), which in emergent combination realise reconstruction of the elementary particles and jets involved in a collision process.

3.3 Gaseous Detectors

Historically, gaseous detectors were the first to be invented. A gas, mostly a mixture with a noble gas such as Argon, is the active material being ionised by incoming high-energy particles. To separate the cations and anions, an electric field is set up in the gas. Depending on the applied voltage, the detector can be operated in different modes. As most incoming particles do not have sufficient ionising capability to generate a signal, one applies a voltage strong enough to amplify the primary signal. This works by further ionisation originating from the first freed electron and its acceleration to a speed where it ionises more gas atoms, creating more free electrons to be accelerated causing an avalanche. In proportional mode, the measured signal is proportional to the primary ionisation. In case an even higher voltage is applied, the detector signal is no longer proportional to the amount of ionisation in the first place. The detector then counts particles independent of their type and ionisation capability. It is a trade-off between voltage applied and therefore dead time and detector efficiency. There are gaseous detectors for different purposes. Counters, e.g. Geiger-Müller tubes, can detect and count particles independent of their type. Furthermore, there are also gaseous trackers such as multi-wire proportional chambers (MWPC) [33].
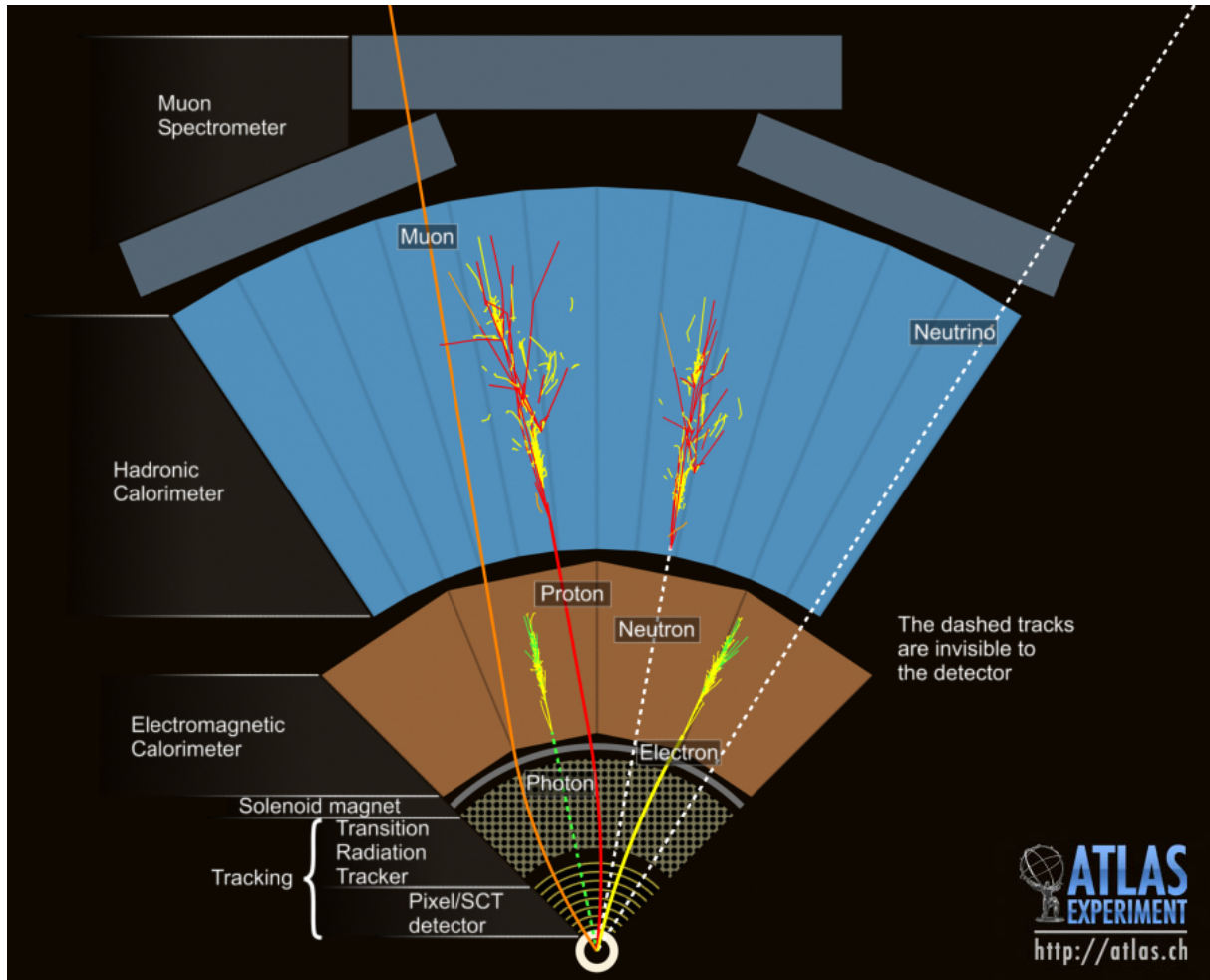
Figure 3.1: Schematic cross-section of the ATLAS experiment ©CERN.

3.4 Calorimeters

Calorimeters determine the energy of a particle. In order to measure the particle's energy, the particle is completely absorbed. There are electromagnetic calorimeters that measure the energy of photons, electrons, and positrons. On the other hand, hadronic calorimeters determine the energy of all hadrons. Both are based on an energetic cascade induced by an incoming high-energy particle, the so-called shower [33]. The hadronic shower is in general more complex than the electromagnetic one. Furthermore, incoming high-energy hadrons also induce an electromagnetic cascade overlapping with the hadronic cascade. As the cross-section for hadrons is smaller than for electrons, the hadronic shower is in general much longer than the electromagnetic in case the incoming particles have the same energy. The longer shower and the more complex cascade are both presented in Figure 3.1.
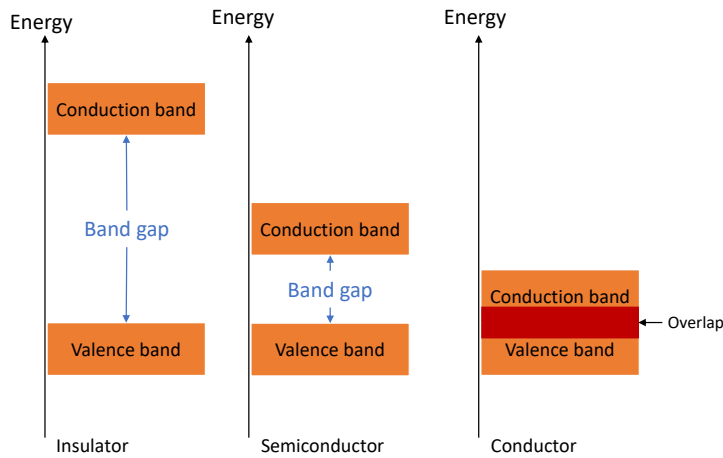
Figure 3.2: Band gap for insulator, semiconductor and conductor.

3.5 Semiconductor Detectors

3.5.1 Basics

Unlike atoms, crystals do not have discrete energy spectra. The energy levels smear to energy bands. A band gap is an energy interval between two bands that can not be occupied in a crystal. The valence band (VB) is completely filled with electrons resulting in its non-conductive behaviour. The conduction band is not or partially filled with electrons. Semiconductors have an empty conduction band at temperature T=0 K but a small band gap [33] as shown in Figure 3.2. The most common and most important semiconductor is Silicon.

3.5.2 Doping

Doping means intentionally putting impurities into a pure semiconductor crystal to alter its electric properties. In order to do so, the doping atoms must have a different number of valence electrons than the intrinsic semiconductor material [33]. There are two types of doping:

n-type doping means that the doping atoms have more valence electrons than the pure semiconductor atoms. Hence, electrons are donated to the conduction band at T > 0 K.
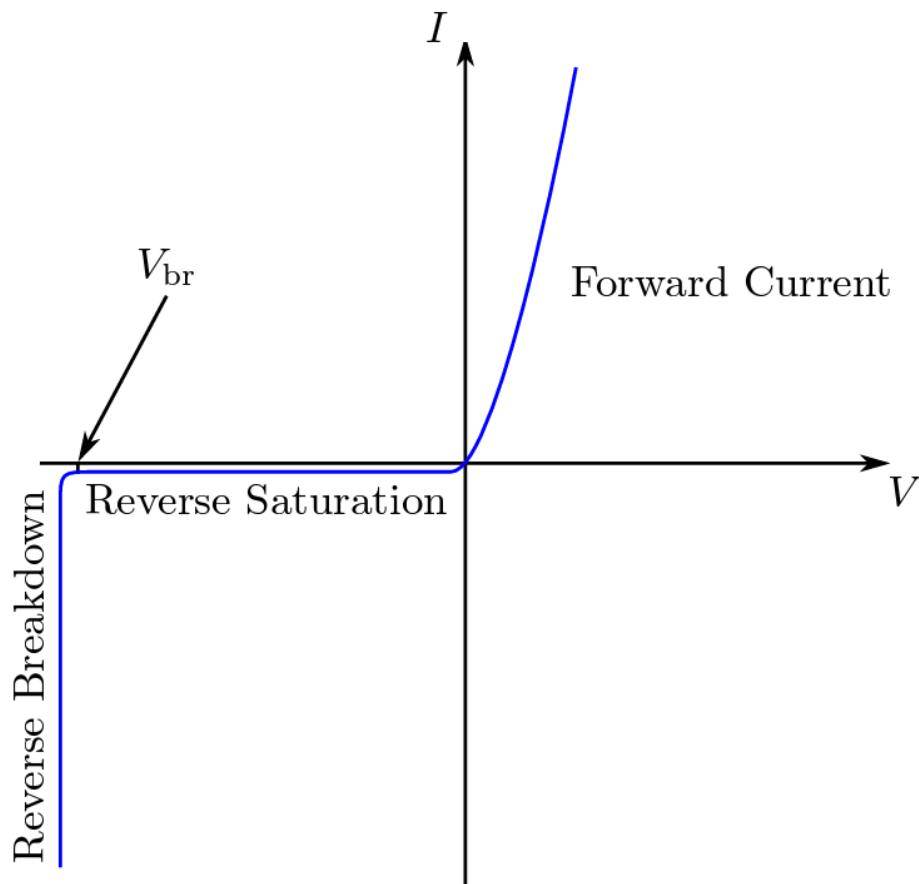
Figure 3.3: Typical I-V curve of a p-n junction [34].

p-type doping   means that the doping atoms have fewer valence electrons such that a hole is created in the valence band. An electron can be accepted to fill this hole.

Doping can shift the Fermi level, the energy level up to which electrons can occupy states at $T = 0\,K$.

3.5.3 p-n Junction

Combining p- and n-type doped semiconductors creates a p-n junction. The diffusion of the electrons/holes causes an electric field between the doped semiconductors, causing a drift in the opposite direction. In equilibrium, both processes balance leaving a depletion zone with a positive and a negative charge at the interface. This depletion region has no free charge-carriers left. One can further apply an electric field to the doped semiconductors. The depth of the depletion zone depends on the number of doped atoms and the applied voltage.

As shown in Figure 3.3, the magnitude of a p-n junction's conducted current strongly

depends on the applied voltage's direction. In reverse bias, the reverse leakage current is comparatively small up to a certain breakdown voltage. The leakage current is approximately constant for a constant temperature but increases exponentially when the temperature rises [35].

3.5.4 Signal Generation

In most cases, the detector material is lightly n-type doped silicon installed between two electrodes that are the source of an applied voltage. An incoming ionising particle creates electron-hole pairs by lifting electrons from the valence to the conduction band since the energy per electron-hole pair excitation is around $3.65\,\mathrm{eV}$ and therefore higher than the band gap ($1.12\,\mathrm{eV}$).

By segmentation of the p-type doped electrode, it is possible to achieve very high spatial resolution.

The measured signal is a current induced by the moving charge carriers. The Shockley-Ramo theorem claims that the induced current is proportional to the applied electric field and to the velocity of the charge-carrying particle [36, 37]. In case an electric field is applied, the charged particles will perform a drift motion directed to the electrodes at an approximately constant drift velocity.

One challenge for signal generation is the separation of signal and background. The background or noise can have multiple sources. The primary source is thermal noise due to the random motion of charge carriers.

3.5.5 Radiation Damage

As semiconductor detectors are often installed near the beam pipe for example at ATLAS, see Section 4.2, they are exposed to a high particle flux and intense radiation. Part of the radiation damage is reversible, while damages from non-ionising energy loss (NIEL) are not. NIEL happens through collisions with the silicon crystal lattice, which lead to vacancies and interstitials between lattice atoms. The collision processes are Coulomb scattering and elastic as well as inelastic scattering of nuclei. High-energy nucleons and nuclei can kick an atom out of its crystal lattice. If enough energy is transferred, the kicked-off atom can kick further atoms off the lattice creating a cluster of radiation damage in the lattice. Different particles cause a different amount of vacancies. Although the average energy transfer for protons is much smaller than the one for neutrons, protons are responsible for many more vacancies, because the cross-section for coulomb scattering is much larger than the cross-section for (in-)elastic neutron scattering. As a consequence,

protons and electrons create more point defects than neutrons. Due to the kicked-out atoms leaving more holes in the lattice, first, the doping concentration can change thus might subsequently lead to type inversion from n-type to p-type doped semiconductor.

4 Background

4.1 The LHC

The *Large Hadron Collider* (Lhc) at Cern in Geneva, Switzerland is the largest and highest-energetic synchrotron particle accelerator built underground mostly to collide protons. Running at a centre-of-mass energy of up to $\sqrt{s} = 13.6\,\text{TeV}$, this accelerator is the key to new high-energy physics. The collider has 4 crossing points for the counterrotating beams each with $7\,\text{TeV}$ if all HL-Lhc upgrades are installed [38]. The Lhc primary collisions are proton-proton, but it is also possible to accelerate heavy ions. Proton-lead and lead-lead collisions are typically performed one month a year.

4.2 The ATLAS Experiment

Atlas (A Toroidal Lhc Apparatus) is one of the main experiments located at the Lhc at Cern. Atlas was one of the two experiments involved in the discovery of the Higgs boson in 2012 [39, 40]. It is the biggest and one of the most complex detectors ever built to test the predictions made by the Standard Model and to search for new physics beyond the Standard Model (BSM). The Atlas experiment is structured in multiple concentric detection layers as shown in Figure 4.2, making it a multi-purpose detector [41].

4.2.1 Muon Detector

The outermost layer of Atlas is the Muon detector. Because of the little interaction of muons with matter, muons leave all other layers. These leptons are detected based on the muon tracks magnetic deflection in a strong magnetic field provided by three large superconducting air-core toroidal magnets presented in Figure 4.1.

4.2.2 Calorimeter

Atlas features a sampling electromagnetic calorimeter (ECal), meaning that the active and passive detector mediums are distinct. For Atlas ECal, the active medium is liquid
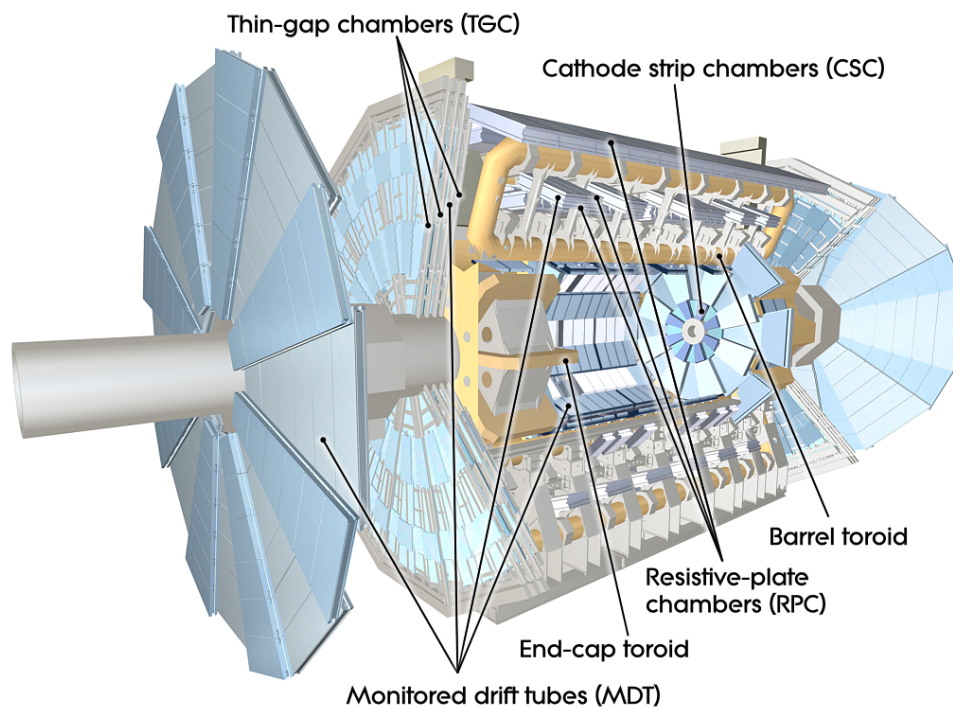
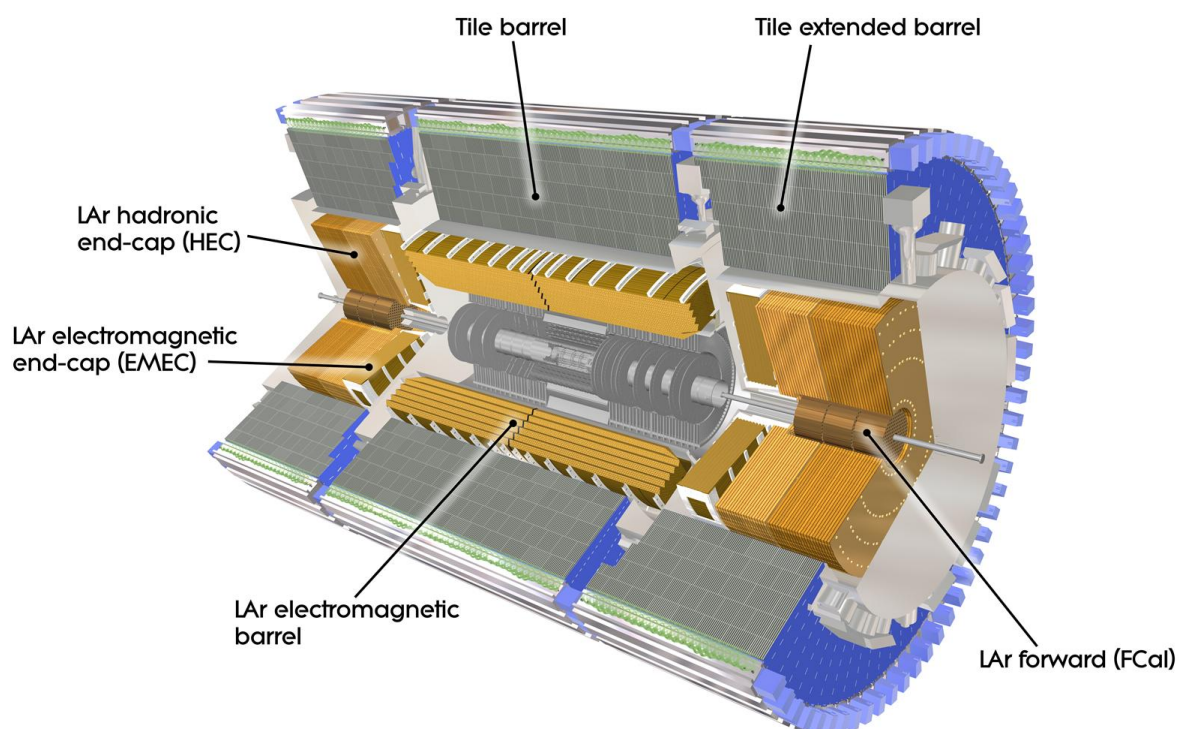*Figure 4.1:* ATLAS muon detection system ©CERN.

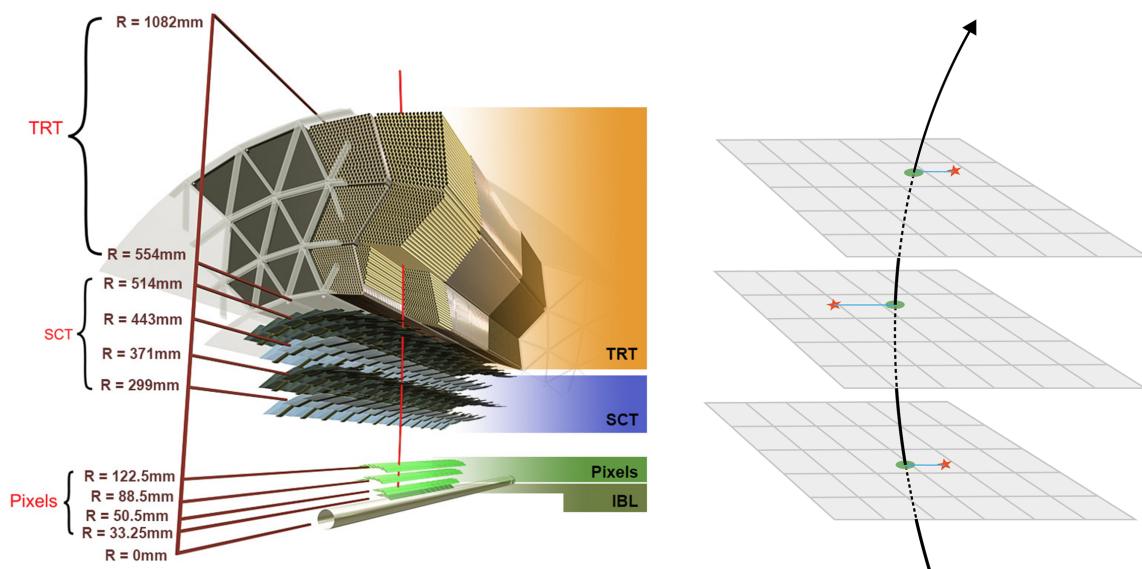*Figure 4.2:* Overview of ATLAS calorimeter system ©CERN.

Figure 4.3: Schematic of ATLAS Inner Detector ©CERN.

Argon (LAr) and the passive medium is a Lead absorber.

The hadronic calorimeter's (HCal) active material is LAr at the endcaps and scintillating tiles for the barrel part. The hadronic calorimeter's passive material is a steel absorber. Furthermore, the forward calorimeter has Copper as its ECal passive medium and Tungsten as HCal's passive medium. LAr is also the active material for the forward calorimeter. Figure 4.2 shows the calorimeter systems of ATLAS.

4.2.3 Inner Detector

The Inner Detector (ID) system consists of multiple layers of modules as shown in Figure 4.3. The inner tracker is finely segmented to obtain the desired angular resolution close to the beam pipe. It is necessary that the inner tracker has a high resolution, as the exact measurement of vertices and interaction points is a mandatory criterion for the identification and reconstruction [41]. The ID includes three sub-detectors:

Pixel Detector is the first point of detection as it encircles the beamline with a radial distance of just 3 cm. The Pixel Detector features four barrel layers of highly granulated silicon detectors. In total approximately 100 million pixels determine the origin with a precision of almost $10\,\mu$m as well as the momentum of the particles.

Semiconductor Tracker (SCT) surrounds the Pixel Detector. Its purpose is to detect and reconstruct the tracks of charge-carrying particles, that are produced in the collision

process. The SCT consist of millions micro silicon detectors spread over more than 4,000 modules resulting in at least 4 silicon crossings for each particle. In consequence, the SCT has a high resolution realising a precision of up to $25\,\mu$m.

Transition Radiation Tracker (TRT) is the ID's outermost layer. It is made up of 300,000 drift tubes ("straws"). Each straw is filled with a gas mixture that is ionised as a charged particle crosses through, creating a detectable electric signal. The particle's track can be reconstructed as it passes through many straws, and the particle's type is identified by transition radiation. Via transition radiation it is possible to separate for example kaons and pions on high energy scales [42].

Figure 4.3 provides a schematic overview of the innermost layers of Atlas.

4.2.4 Trigger

With a collision frequency of $40\,$MHz [38] and more than 600 million inelastic events per second, the amount of data taken at Atlas is too much even for state-of-the-art computing. Moreover, most of the events happening are well-known and not of interest. Therefore Atlas uses a multi-layer trigger system. The triggers filter the interesting events either at the hardware or the software level, such that a reasonable amount of data is transferred and stored for data analysis. In total, the trigger system reduces the event rate from $40\,$MHz to $1000\,$Hz with which the data of the events is stored at the Cern data centre for further investigation.

4.3 ITk Pixel Detector

The current ID system will be replaced by an all-silicon Inner Tracker (ITk). Currently, the ITk project is in the preproduction phase. Besides the outer barrels and the outer endcaps, there is a replaceable inner barrel system. All of them are made up of more than 9000 modules (thin Silicon and FE chips). The majority of these modules are n-in-p planar quad modules, meaning, that there are 4 chips per module. These chips are called RD53C. To allow high precision, each chip is segmented into 384×400 pixels making a total number of 153,600 pixels. They comprise a hybrid design, which means, that the sensor is directly connected to the readout electronics via small metal bump bonds. The whole detector system is cooled with CO_2. Moreover, the ITk has an advanced serial powering system, which together with the reduced number of readout cables, optimises the total number of cables in the inner detector regions. As high voltages can be applied to the sensors, a large depletion zone is possible.

5 Module Assembly

The modules for operation in ITk must guarantee 10 years of service in the ATLAS experiment.

Ideally, all quad modules should be comparable in dimension and electrical functionality. This assumes equal module building procedures, quality and prerequisites in all institutes despite the strongly decentralised module production. Building a module means that the flexible electronics (the flex) with its surface-mounted devices (SMD) components is glued on top of the bare module (BM). The BM consists of the front end chips (FE) that are bump bonded to the sensor and finally, the wire-bonding enables the communication between the chips and the flex.

To achieve a common module assembling procedure, a module assembly tool was designed and manufactured in the II. Institute of Physics in Göttingen. Thus, the II. Institute of Physics in Göttingen is not only a site for module production but also for assembly tool production, distributing assembly tools to ITk institutes all over the world. In Göttingen, layer 2 (L2) quad modules of $150\,\mu$m sensor thickness are assembled before testing them. The procedure is well defined by the ATLAS module site qualification (SQ) [43–45].

5.1 Metrology

Since the modules are required to have identical dimensions, their components, the flex and the bare module (BM) are inspected under a microscope in metrology before the assembly. Furthermore, several spots and distances are measured, to monitor the flatness of the sensor and to ensure, that the components meet the requirements and to report production abnormalities. For example, the check of the power adapter inputs' height and dimension is part of metrology. Metrology also covers a check for production impurities. For the BM this includes chipped corners, poor dicing and rough edges of the sensor, tooling marks, scratches and contaminations such as dust. The flex is checked for irregular dicing, bond pad contaminations, scratches, chipped inner corners and excess material. On top of the component's dimensions, their weight is also determined using a milligram

precise scale.

The requirements that the components have to meet are well defined in the table with specifications on x-,y-, and z-dimensions of the BM, the flex and the assembled module in [46, 47].

Furthermore, the metrology assures that the assembling tool works properly, since it requires the components to precisely meet the dimensions.

5.2 Glueing

The assembly tool mentioned above is mainly relevant for the precise glueing of the module meaning for the combination of the two components, whose dimensions are precisely verified in metrology. The assembly tool includes two jigs, whose holding is vacuum supported, one to hold the flex, the other one for the bare module. This tool allows a $50\,\mu$m precision when it comes to the centering of the module and the flex thanks to highly precise rods and ball bearings that slide into each other. This micrometre precision must be fulfilled for wire-bonding. A stencil in combination with a spatula distributes the 2-component glue on the bare module before the two jigs are put together. Once the two components are agglutinated, the glue has to cure for 8 hours. The weight of the cured glued module is measured and the weight of the glue is calculated with the data of the flex and the BM taken in metrology.

After the glueing, metrology is performed on the cured module to determine the centering of the flex and the BM and to assure the adhesive thickness of $(40 \pm 15)\,\mu$m.

5.3 Visual Inspection

The visual inspection (VI) is for cross checking the quality of the module. The high definition photos that are taken with a camera, are checked for pad contamination, particulate contamination, watermarks, scratches, soldermark spills, component misalignment and short or close proximity. All those criteria are weighted equally to determine an overall grade for the inspected module. In case any of the criteria are not met, the module is separated into 16 segments, to classify where exactly which anomalies are located.

5.4 Wire-bonding

The last step that is performed in Göttingen is the wire-bonding. About 200 thin Aluminium wires are bonded to connect the chips and the flex. Moreover, a pull tester
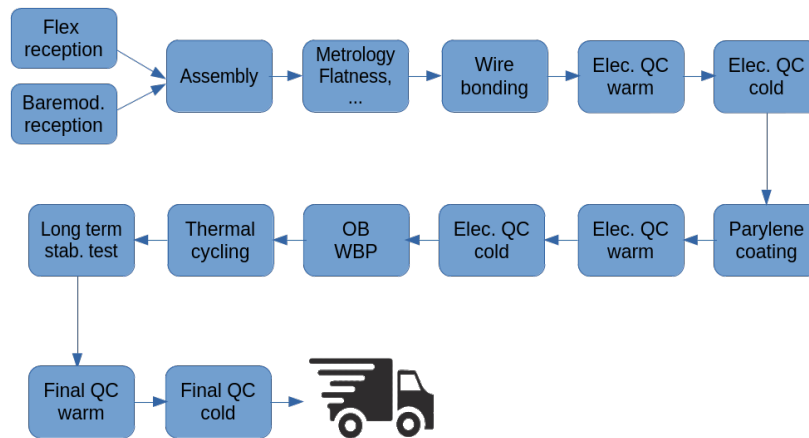
Figure 5.1: The schematic production flow for the ITkPix quad modules.

determines the force it takes to cut the wire-bonding on certain connections that were previously wire-bonded with the purpose of demonstrating the bonding quality.

After the wire-bonding a first electric quality control (QC) is performed before the modules are sent to parylene coating. Figure 5.1 shows schematically the production flow chart.

5.5 The Carrier

Most of the time, the modules are stored on a local support carrier, a protection, transport and storage case for the module as shown in Figure 5.2. This carrier features a plastic top shield (plexiglas lid) and a metal frame. Everything is screwed to the bottom plate of the carrier. The carrier has two output lanes for the two types of connection flexes, which are called pigtails, one for the power, and one for the data acquisition. In between the tests, all carriers are stored in the dry air flooded climate box. Once the module assembly is completed, the module does not need to be taken out of the carrier.
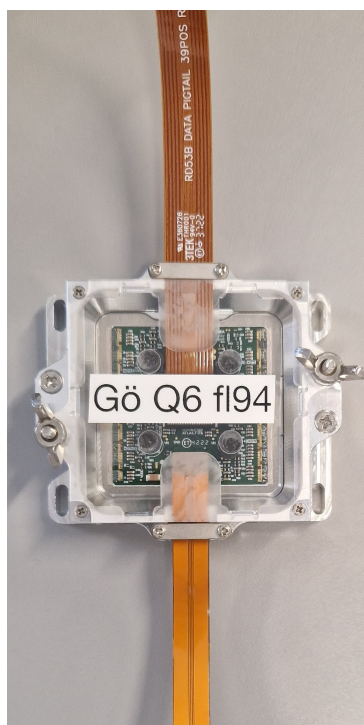
Figure 5.2: One of the modules in the carrier.

6 The Test Setup

To be able to perform electrical tests on the modules, a suitable setup in the laboratory is mandatory. The local setup is designed for parallel (semi-)automatic testing of multiple modules.

6.1 Source Box

The local setup used for this thesis work is housed in a stainless steel box to completely shield the outside world from radiation originating from inside the box. At the top of the source box, a motorised source holder with a remotely controlled shutter is installed. Its position can be adjusted remotely via a PC within the range of the rails that cover nearly the whole box. For a source scan, presented in Section 7.5, the shutter opening has to be aligned with the module such that the source is positioned about $20\,\mathrm{cm}$ above the module. Thus the cone of irradiation covers the whole module.

At the bottom of the source box, there are two setups for electrical testing at different temperatures, specified in Section 7. Referring to the temperatures in which the electrical tests, that are presented in the next Chapter, are performed, the setups are called cold and warm setups.

The cold setup comprises a foam box for thermal insulation. Inside the foam box in the source box, three components of the cooling and test system are stacked. The cold plate, cooled by an external silicone oil chiller (Huber unistat 705), is the ground for a Peltier element. A Peltier element is a semi-conductor element that can regulate the temperature. A vacuum chuck to hold the module is placed on top of the Peltier element, as illustrated in Figure 6.1. In symbiotical combination a precise temperature control is realised, that cools the module to the test temperature of $-15\,\mathrm{°C}$.

For cold tests, the module is placed in the frame of the carrier without the bottom part on the vacuum chuck of the cold setup (see Figure 6.2), to secure its contact with the cooling unit to ensure heat dissipation when powering up the module. The temperature, humidity and dewpoint are monitored at multiple points of this setup: two Pt1000 sensors

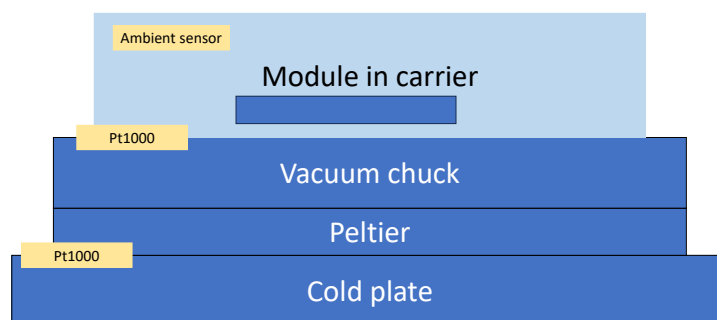***Figure 6.1:*** Schematic of the cold setup inside the foam box in the source box.
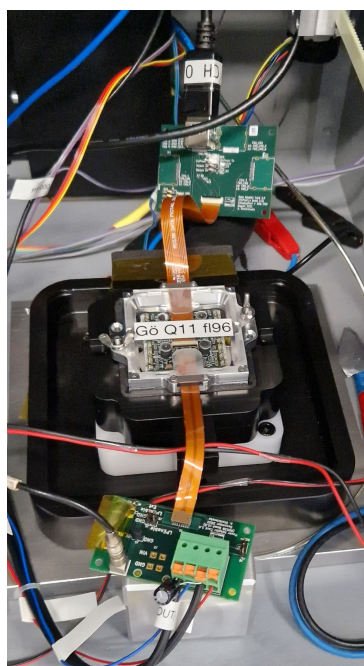

Figure 6.2: One of the modules in the frame of the carrier without the bottom is placed on the vacuum chuck of the cold setup. The slightly bigger PCB board in the back is for data acquisition, and the smaller PCB board in the front is for power.

determine the temperature on the cold plate and on the vacuum chuck. An ambient sensor monitors the temperature as well as the dewpoint directly on the module. When cooling the module down to $-15\,°C$ for the cold test the dewpoint of the surrounding air is reached. To avoid any kind of condensation or freezing that can damage the module and the test setup, there is a dry air supply, that goes directly in the module carrier. Thus, the relative humidity in the direct module surrounding reduces to less than 1% and the dewpoint inside the foam box drops to less than $-40\,°C$. The vacuum is monitored with a sensor for vacuum pressure (SMC ZSE30A) outside the source box.

The electrical communication to the module is achieved by two pigtails, one data and one power pigtail. The pigtails connect the module with the power adapter board and the data adapter board. Power and module temperature are controlled via the smaller printed circuit board (PCB), data acquisition is done via the bigger adapter board shown in Figure 6.2.

The monitoring of the temperature and ambient sensors, as well as the vacuum monitoring routes in an Arduino Mega, which is run with LABREMOTE, a common ITk software package. The Arduino has a USB connection to the DCS PC. On the PC, the YARR readout software is used. The PC also is in command of the three power supplies. One for biasing the module, one for powering the chips and a third one for powering the Peltier element. The temperature monitoring and cooling are assisted and maintained by an interlock, that in case of problems e.g. overheating stops the process.

With this setup, all temperatures that are necessary for module qualification (QC) can be reached. Nevertheless, there is a second setup for warm tests only, whose cooling is simpler and more reliable.

The warm setup, next to the cold setup, is a second setup for warm tests only. This setup features a power and a data adapter board just like the cold setup both are connected to the readout PC. The difference is the cooling, which is satisfied with two remotely powered fans. For electrical warm tests, the carrier with the module in it is installed on the heat distributing platform.

The power supply features three electrical power sources, one for high voltage (HV), one for the low voltage (LV) power supply for the module and a third one for the Peltier power supply. The HV is set to a nominal value of -100 V, for the biasing/depletion zone. The LV is set to 3.6 V which is a higher voltage than the required input voltage (V_{in}) on the power adapter board. The higher value of 3.6 V respects the voltage drop within the cables leading to the module. This power supply operates in constant current mode,

meaning the current is stabilised at 5.88 A. All Power sources are remotely controlled via a PC.

The interlock stops the module powering once the temperature gets too high, for example in case the cooling system fails. Or if the dewpoint, which is monitored via the module and the surrounding temperature and humidity gets too high to avoid condensation on the module itself or on the vacuum chuck.

7 Scans and Tests

The key points to ensure the operational quality of the modules are the electrical tests and scans performed to verify the functionality of the chips.

Warm and Cold Tests

Concerning the testing, cold and warm tests are differentiated. This refers to the temperature the module is cooled to during the performance of the test. Warm tests are performed with a module temperature of 20 °C whereas cold tests are performed in an environment of −15 °C. In both cases, the module has to be cooled because otherwise, its power consumption heats the module quickly. The test setup described in Section 6.1 provides the needed cooling.

To operate a module, firstly its configuration (config) files are generated. The config files steer the modules. For each module, three config files are generated, one for the warm tests, and one for the cold tests and one for low power mode.

7.1 First Power-up

The first electrical test for a module is the first power-up. The module is powered up with the nominal current of 5.88 A. Since a quad module has four chips in parallel, each of them has an input current of 1.47 A. For this test, the input voltage on the power adapter card is measured using an external multimeter. A module passes this test if the input voltage is (1.757 ± 0.025) V.

7.2 Digital and Analogue Scan

These two tests verify the basic operation of all pixels. The module comprises a purely electrical digital part and an analogue part. The chip can inject charge into the analogue and in the digital part of the module. Usually for YARR, 100 signals are injected. The number of trigger signals is predefined and serves as a reference for the scanned occupancy.

The digital scan tests the purely digital part of the chip. Since this part is not prone to error a perfect scan response is expected. If this is not the case, further investigation is needed on the digital part of the module as well as the readout, to check all connections and circuit components.

The analogue scan tests the analogue part of the chip. As this part is subject to noise such as thermal noise, some pixels might not show the perfect response from the digital scan.

Since YARR injects a signal 100 times per pixel, a pixel is labelled "good" if its number of hits is in the range between 98 and 102. In case a pixel measures more than 102 or less than 98 signals, the corresponding pixel is labelled "bad". These pixels are excluded from the measurements, which is called masking.

The last possible result is that some pixels show no hits in the analogue scan. These pixels are called "dead". Dead pixels occur for example when the module is mechanically damaged.

7.3 Threshold Scan

All sensors have an adjustable threshold that is set to a fixed value. A threshold is a minimum amount of charge that counts as a hit. The threshold is given in units of elementary charge.

As not every electron, that is randomly ionised, should be counted as a signal, the threshold is set to a certain value high enough that it is only reached by incoming high energetic ionising particles. Below this defined threshold, the discriminator in the chips suppresses the noise that occurs.

The threshold scan probes the value of the threshold for every pixel.

7.4 Tuning

To achieve a Gaussian distribution around a desired value, the threshold of the module is (re-)tuned. The calibration of the programmable registers is done globally and pixel-wise, which correspondingly is called global and pixel (re-)tuning. The global (re-)tuning sets the global, so the general threshold to the desired value. The pixel (re-)tuning improves the threshold of the single pixels and aims to fix the threshold values, especially for the pixels on the edges of the threshold distribution.

First of all, the global, so the general threshold is set to $2000\,\mathrm{e}$. After also performing a

pixel tuning to this value, the next step is to perform a global retuning to 1500 e followed by a pixel retuning to the same value. This is a smaller and more realistic value for the threshold.

7.5 Source Scan

To test the module with real ionising radiation, a source scan is performed. All tests and scans presented so far only involve the chip. The source scan tests the sensor too. A ^{90}Sr source is installed in the motorised source holder described in Section 6.1. ^{90}Sr is a β^- source, which means that the source emits electrons. The emitted electrons have a maximal energy of 546 keV [48]. The activity of the source is in the magnitude of MBq. The source scan sends a trigger signal of a fixed frequency and counts the hits that occur. When starting the source scan, the duration of exposure can be adjusted. By the parasitic capacitance, the bump bond connection can be detected. Other sites use different radioactive sources or X-ray sources for this scan.

Selftrigger Source Scan The standard source scan does not profit from the high activity of the source. Triggering of a fixed frequency is not the most efficient way to perform the source scan. The RD53B chips have a selftrigger feature. The selftrigger method sends out a trigger signal whenever a hit is recognised, securing at least one hit per trigger signal.

7.6 Noise Scan

As briefly mentioned above, not all pixels will have the defined number of hits in an analogue scan. The noisy pixels register hits without a signal. Such pixels are labelled "bad" in an analogue scan and are masked using a noise scan. After masking, problematic pixels do not occur in the occupancy map in the further tests. As a consequence, noisy pixels do not influence their neighbouring pixels' results.

7.7 Disconnected Bump Scan

A continuous problem resulting from the hybrid design of the detector are disconnected bumps. Usually, the small metal bumps connect the chip and the sensor. The connection is created by melting the metal bumps to permanently connect sensor and chip. When

the bumps are disconnected, the electric charge can not be processed. As this limits the functionality of the module, it is important to know if any of the four chips has disconnected bumps. To find out, the disconnected bump scan is performed.

The disconnected bump scan detects disconnected and broken bumps such as the "dead" pixels from an analogue scan. For disconnected bump scan, the capacitive behaviour of a pixel is probed when injecting charge in the neighbouring pixels. A pixel with disconnected bump will not see the influence of the charge injected in the neighbouring pixels. Thus, the detection works indirectly, via the pixels crosstalk.

7.8 Electrical QC

For the module QC, several tests have to be performed on the module. Summarised in a bash script, these tests run automatically.

ADC Calibration The analogue-to-digital converter (ADC) must be calibrated. In this step, the analogue signal and the digital output of the chip are aligned. Different known amounts of charge are injected into the module and its response is adjusted to the right values. This results in a linear dependence.

A chip passes if the linear function has a slope of (0.187 ± 0.037) mV/LSB (least significant bit), a calibration offset of (11 ± 20) mV and a calibration linearity of (0 ± 4) mV. After the ADC calibration is performed, all chip internal voltages and currents can be used as a reference, so no external multimeter is required like in the wafer probing.

SLDO The shunt low dropout voltage (SLDO). This test checks, that after the configuration all chip internal currents and voltages are within the nominal operation range as defined in [49]. Also, it is verified that the input voltage (V_{in}) for the digital and analogue parts of the module do not differ by more than 0.01 V. The SLDO voltage regulator is implemented in the chip so that the chip can adjust the digital and analogue voltages it needs from a power supply in constant current mode. Furthermore, this feature finds the operation point for each chip, which is especially relevant in the serial powering of multiple modules.

VCAL Readback This test cross-checks and updates the chip's internal calibration voltage (VCAL), which is used for example for the tuning. It is scanned, if the current-voltage characteristic (I-V curve) follows the expected linear behaviour. Thus, the pass

criteria are a calibration slope of (0.2 ± 0.04) mV/LSB, a calibration offset of (-3 ± 20) mV and a calibration linearity of (0 ± 4) mV.

Injection Capacitance This test cross-checks and updates the injection capacitance. To pass this test, the injection capacitance must be (7.87 ± 1.13) fF.
In combination with the VCAL the injected charge is determined.

Analogue Readback This test verifies all chip internal voltages and currents. To pass this test a list of criteria must be fulfilled e.g. certain voltages for the temperature sensors. In all details the values are presented in [49].

Low Power Mode This test probes the module functionality in low power (LP) mode, meaning in a mode in which the voltage drops under the nominal voltage and the current drops to a lowered current, the nominal LP mode current. For this test $V_{in}^{analogue}$ and $V_{in}^{digital}$ are measured, to see if they are within the required range.

Overvoltage Protection This test makes sure that the overvoltage protection mechanism works properly. Therefore, the V_{in} must be in a range of 0.04 V around the theoretical value, for a given current. Moreover, this test checks if certain currents and voltages in low power mode (LP mode) match the reference values.

8 Results

Within the scope of this thesis, three fully assembled pre-production modules (ITkPixV1.1) are tested in terms of their electrical properties, which are part of electrical QC. These three modules are called Q6, Q11 and Q12. On each quad module, there are 4 chips, whose names follow a hexadecimal encoding (hex code). Normally, the chips are positioned counterclockwise with increasing hexadecimal labels. With this numbering, one can refer to the single chips on a module, since the tests presented above give chip wise results and not just one result for the whole module.

Module Q6 had one and later two completely failing chips in the warm test. This is the reason why for every warm test performed on Q6 there are no more than 3 out of 4 chip results. In the cold tests, even more chips fail so it was decided to not proceed with cold testing on this module.

  Since readout problems occurred on Q11, as shown in Figure 8.1, 8 columns, with 384 pixels each are disabled. For this reason, there are at least 3072 "failing" pixels on one of the chips. This circumstance is discussed in detail in Section 9.

The module Q12 is a module from the Physikalisches Institut of University of Bonn. Their results are cross-checked to verify the BDAQ data acquisition system which was used by the Bonn scientists. For this cross check it is sufficient to perform the tests warm. Also, the cold testing with Q12 was stopped since a failing chip in the cold test was noticed (see Table 8.2).

First Power-up Result   The measured input voltages on the power adapter card are listed in Table 8.1. Not all of them are in the range of $(1.758 \pm 0.025)\,\mathrm{V}$.

Table 8.1: Results of the first power up for the three tested modules at the different test temperatures.

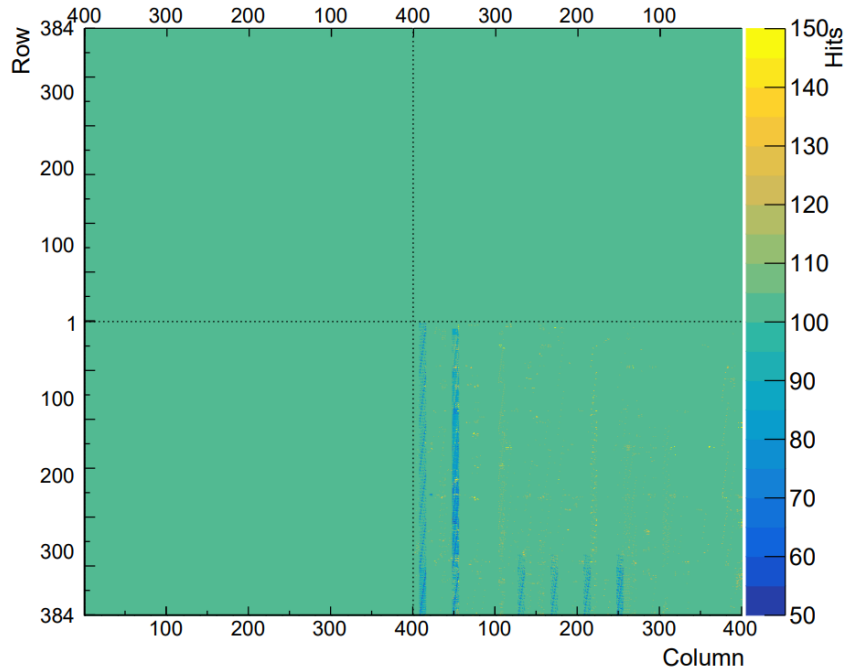| Module	V in	passes QC
Q6, warm	1.704 V	X
Q11, warm	1.689 V	X
Q12, warm	1.772 V	✓
Q11, cold	1.680 V	X

Figure 8.1: Before disabling 8 columns, a problematic periodic readout pattern occurs on one of the chips of Q11.

8.1 Digital and Analogue Scan

Digital Scan Most of the chips show the expected flawless result. Figure 8.2 shows an example of a perfect digital scan, where the occupancy map shows only the 100 trigger signals. On module Q11, the chip with the disabled columns has 3072 failing pixels from the disabled columns. Figure 8.3 shows the digital warm scan for this module.

Analogue Scan The analogue scans show a certain number of failing pixels. One example of an analogue scan occupancy map is presented in Figure 8.4. Table 8.2 shows the number of failing pixels in analogue scan for all modules.

8.2 Threshold Scan and Tuning

Before the tuning, the threshold distribution of all chips does not follow an expected Gaussian distribution.

Usually, the value is set to about $2000\,\text{e}$ before tuning. After the retuning, the threshold distribution is much sharper around the desired value of $1500\,\text{e}$. Figure 8.5 shows one typical example of the threshold distribution before and after the tuning. Note, that of course not all chips and all modules show the exact same threshold distribution in terms
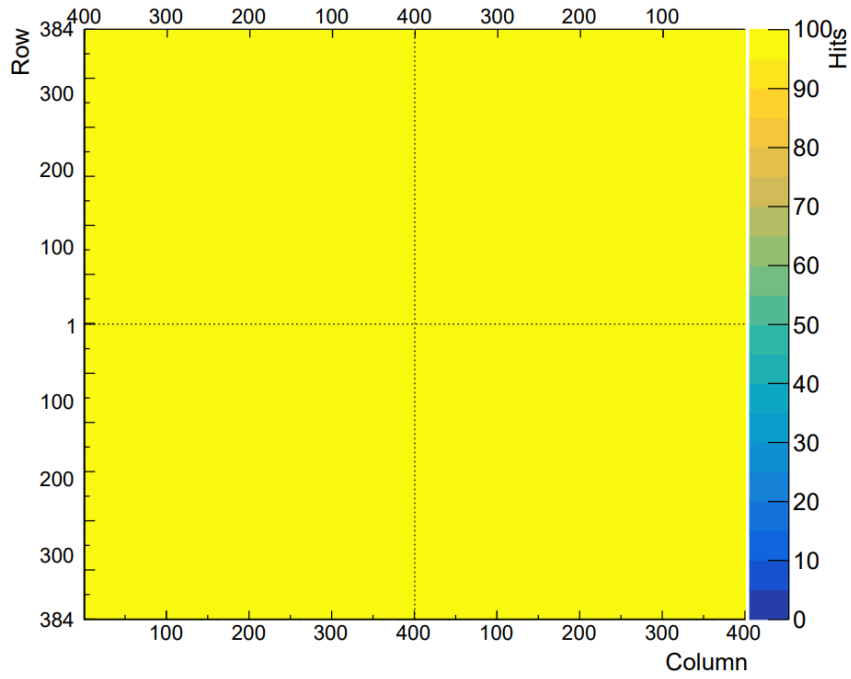
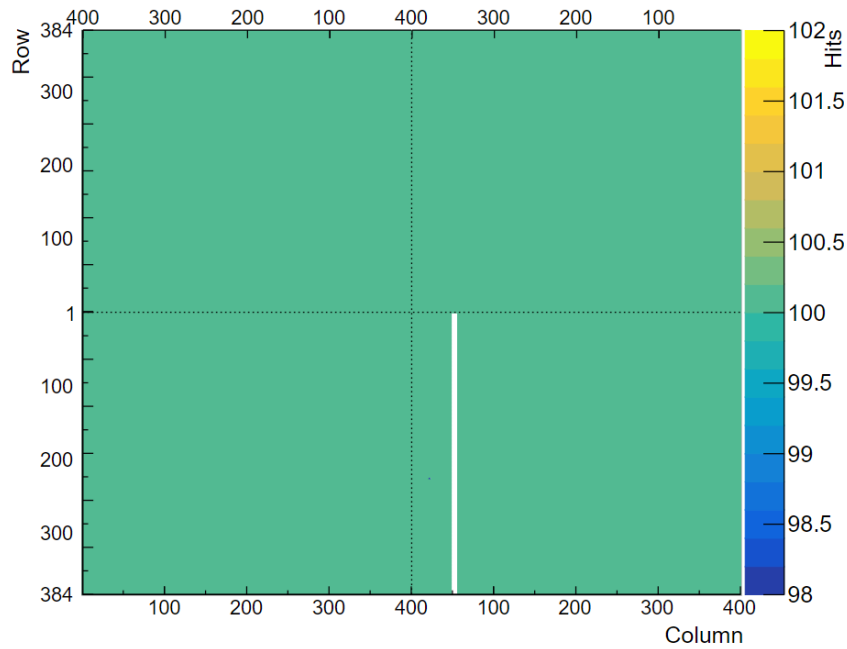***Figure 8.2:*** Occupancy map of a digital scan of Q12 in a warm test environment.

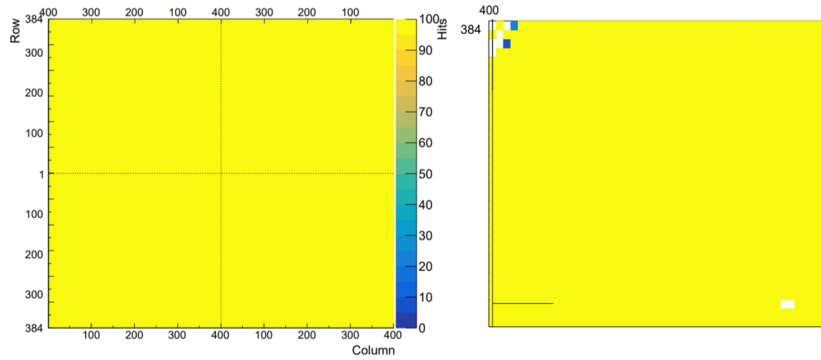***Figure 8.3:*** Digital scan after disabling 8 columns on one of the chips of Q11.

Figure 8.4: Occupancy map of an analogue scan of Q12 in warm test environment. The total number of failing pixels according to Table 8.2 can be found especially on the left edges. On the right, a zoom-in on the top left corner of the occupancy map shows some of the failing pixels.

Table 8.2: The number of failing pixels in analogue scan for the three tested modules at the different test temperatures. The 4 numbers represent the number of failing pixels on each of the 4 chips, in hex order. Q6 only had 2 working chips, when the scan was performed. The high number of failing pixels on one of the chips of Q12 in cold analogue scan originates from the failure of this chip in cold tests.

Module	number of failing pixels
Q6, warm	23, 1
Q11, warm	2, 3084, 3, 5
Q12, warm	171, 1, 98, 25
Q11, cold	6, 3092, 10, 6
Q12, cold	61, 54750, 2, 1

of the numeric values of the distribution, but qualitatively their behaviour is the same.

8.3 Source Scan

Source scans of different durations of exposure were performed. As expected, the longer the source scan runs, the more hits are recognised by the sensor just like presented in Figure 8.6.

In general, the selftrigger source scan is much more efficient than the normal source scan. As an example, Figure 8.6 shows a 3 hours-long and a 5 hours-long source scan and Figure 8.7 shows a hitmap and histogram of a 50 minutes selftrigger source scan. It is conspicuous, that the SMD components from the flex are clearly visible in the hitmaps from the source scan. Under the SMD components, the number of hits is much lower than everywhere else. It is barely possible to observe more than 4 hits under the SMD
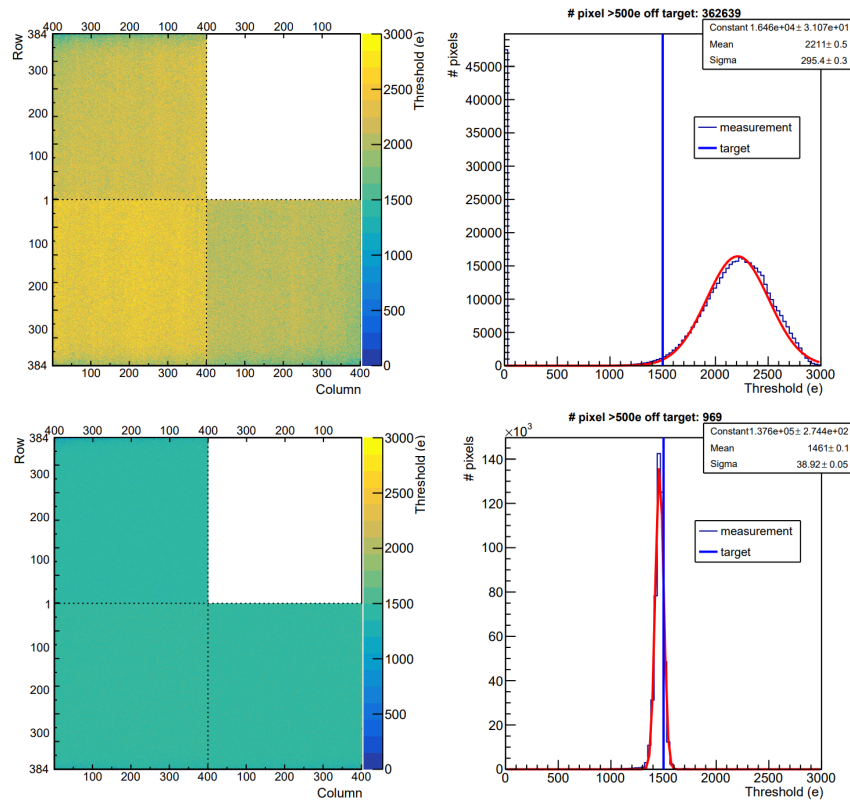
Figure 8.5: Threshold of Q6 warm before and after tuning. The threshold distribution is much sharper around the targeted value.

components, even with the 5 hours-long source scan presented in Figure 8.6.

8.4 Electrical QC

No module passes every aspect of the electrical QC. Some of the tests that are part of the electrical module QC are passed. Table 8.3 shows the results, which module passed which of the electrical module QC tests. One example of a passed ADC calibration is presented in Figure 8.8.
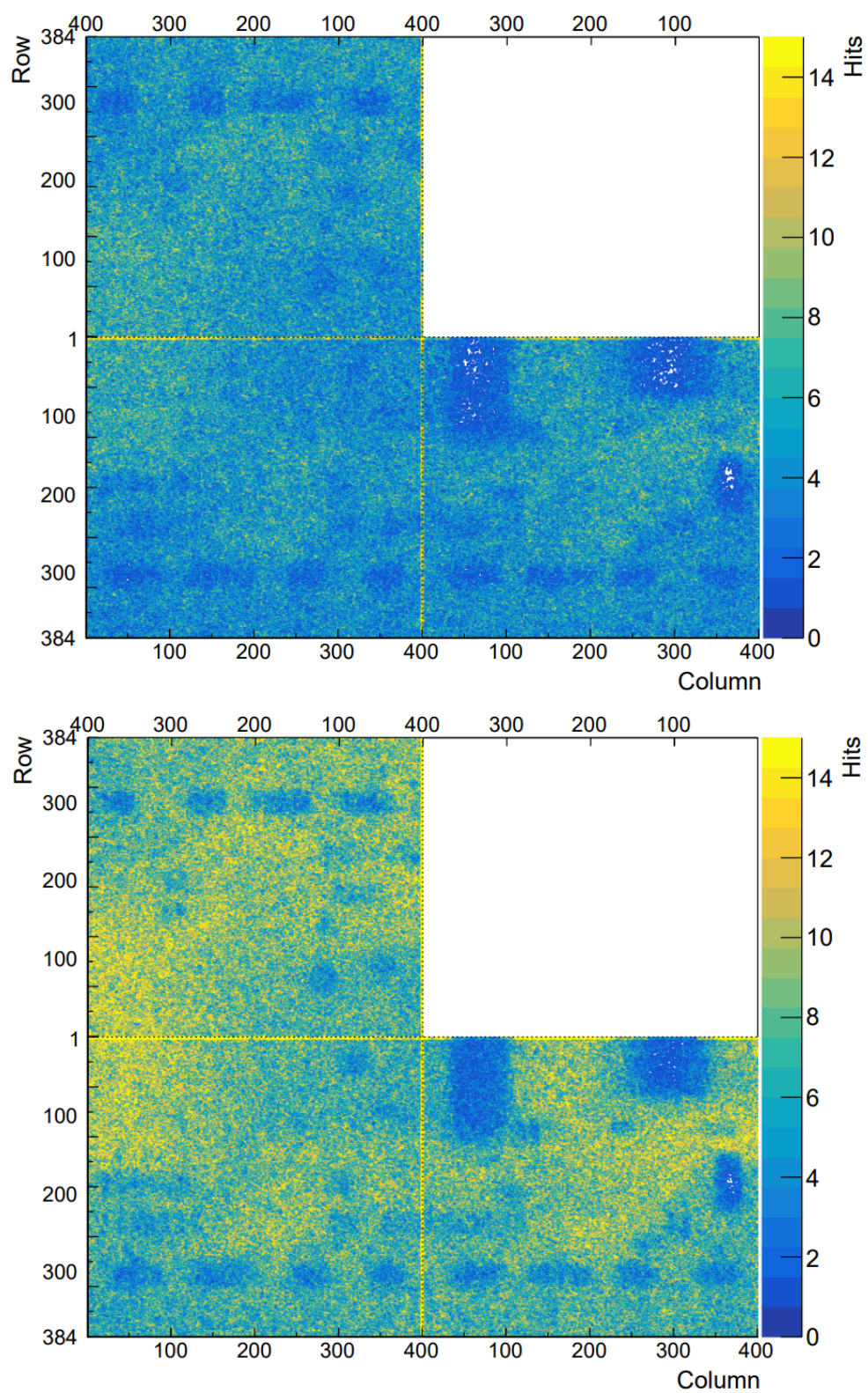
Figure 8.6: Source scan performed on Q6 warm. The first plot shows the hitmap after 3 hours of exposure, the second plot shows a hitmap after 5 hours-long source scan.
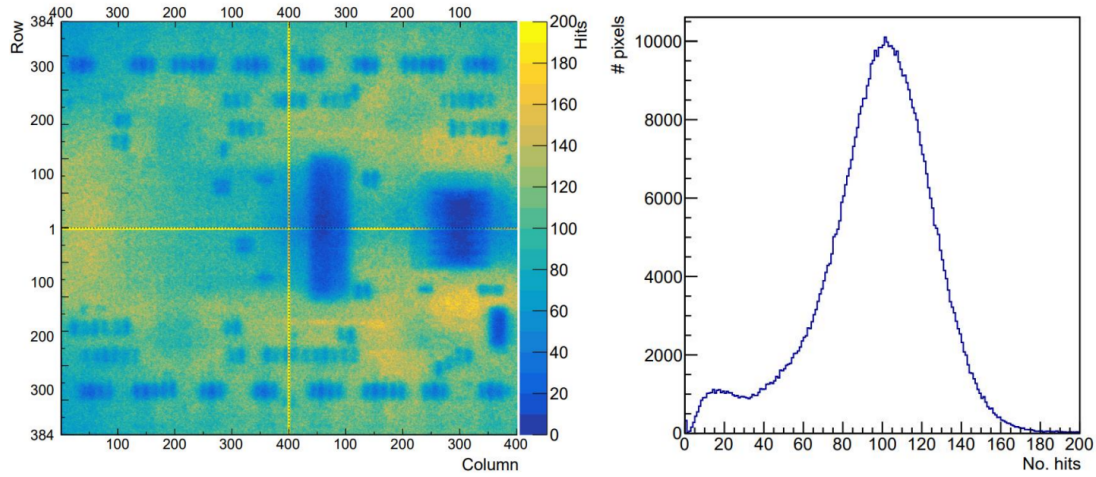
Figure 8.7: 50 minutes selftrigger source scan performed on Q12 warm.

Table 8.3: Results of the electrical QC for the three tested modules at the different test temperatures.

Test / Module	Q6, warm	Q11, warm	Q12, warm
ADC Calibration	✓	✓	✓
Analogue readback	X	X	X
SLDO	X	X	X
VCAL Calibration	✓	✓	✓
Injection capacitance	✓	✓	✓
LP Mode	X	X	X
Overvoltage Protection	X	X	X
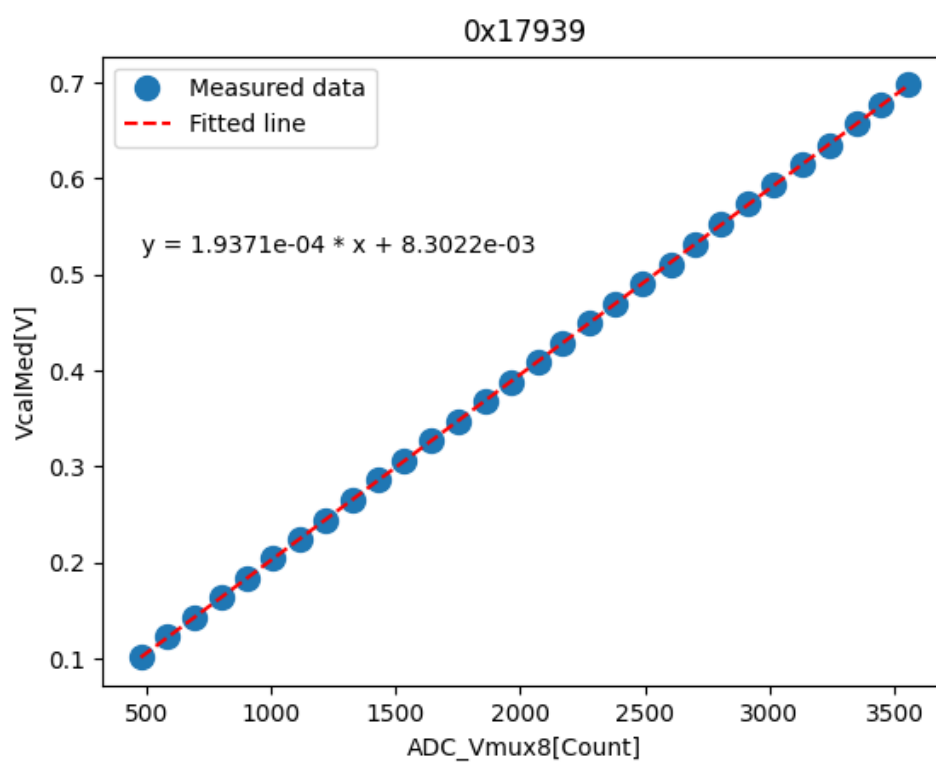
Figure 8.8: Linear function as expected for ADC calibration, performed on Q11 in a warm test.

9 Discussion

At the beginning of the tests, readout problems on one of the chips of Q11 were observed. A regular pattern in the digital scan appeared, as shown in Figure 8.1. This problem originated in at least one of the columns. After disabling the particular 8 columns with 384 pixels each, which is possible in the config file, the regular readout pattern disappears at the cost of 3,072 "failing", disabled pixels. Q11 fails the first power-up test meaning the input voltage on the power adapter board is less than required. The module's proper operation presupposes a sufficient input voltage. It will be tested to increase the current on the power supply with the perspective of realising the nominal input voltage. The electrical tests and scans will be repeated once the nominal input voltage is achieved, to investigate if this is the reason why Q11 fails certain tests.

In order to properly operate module Q12, the voltage on the power supply was raised. Before the voltage was adapted, a pattern in the readout appeared in the digital scan as shown in Figure 9.1. There are two approaches to solving this problem. The first way is to increase the LV from $3.5\,\mathrm{V}$ to $3.6\,\mathrm{V}$ on the power supply. The second way is to increase the current from $5.88\,\mathrm{A}$ to $6\,\mathrm{A}$. Since both approaches solve the problem, the module continued with the first option, because in the future production, modules that do not operate on the nominal current of $5.88\,\mathrm{A}$ will not be installed in the detector. Q12 already showed problematic behaviour in BM IV measurement. The high leakage current might be the source of the problems with this module.

Chips failure in cold tests was already observed before with the previous chips called RD53A. Failing chips in cold tests were observed in many (pre-)production sites. Thus, this was reported and will be further investigated by the whole ITk group.

It appears quite frequently, that the failing pixels in for example analogue scans are close to the edges or corners. This result is compatible with the observation in VI where the majority of scratches or contaminations are found close to the edge or the corner. Scratches, chipped corners or contaminations have a negative impact on the sensor since they are hardware defects that limit the operation quality of the module.
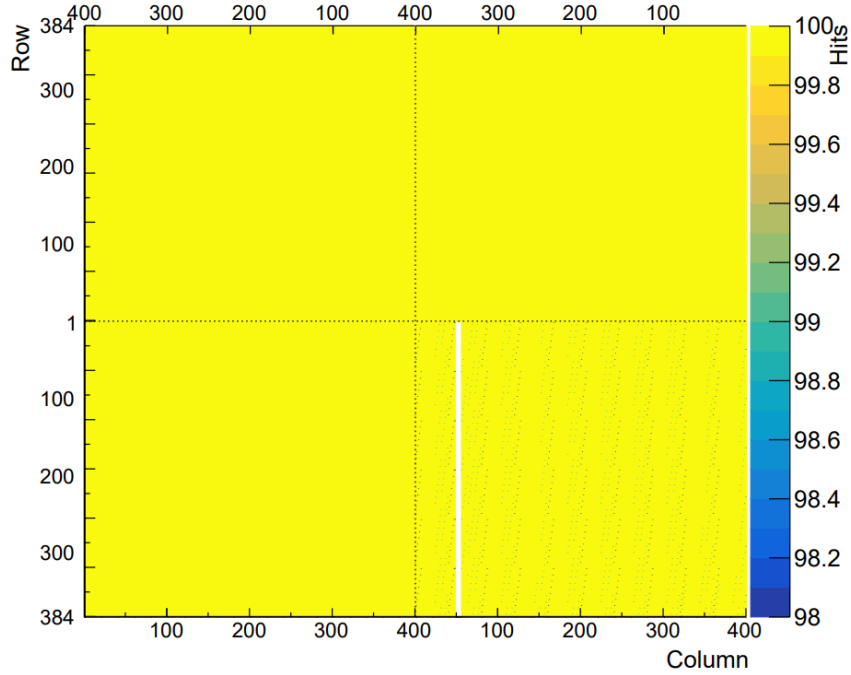
Figure 9.1: Analogue scan performed on Q12 before the voltage was increased.

The electrical QC was not passed in every aspect by any of the modules. For Q6 and Q11 the failed first power-up might be the reason. Since the nominal V_{in} is part of the criteria for certain electrical QC tests, the lower V_{in} on the power adapter board might cause the modules to fail for example the analogue readback. To find out, these modules will be tested again with an increased voltage or current to raise V_{in} to the desired value of (1.757 ± 0.025) V. Q12 did pass the first power-up. Nevertheless, this module fails the same tests of the electrical QC as Q6 and Q11. The increased leakage current of Q12 might lead to the test failure.

9.1 Threshold Test

Since the quad modules that were object to this thesis are L2 preproduction modules, they target a threshold of 1500 e. The primary tuning to 2000 e followed by a retuning to 1500 e gives better results by experience. The result is a more centred Gaussian distribution around the set 1500 e. The tuning and retuning have to be done for both, warm and cold tests since the chips have two different configs for warm and cold tests.
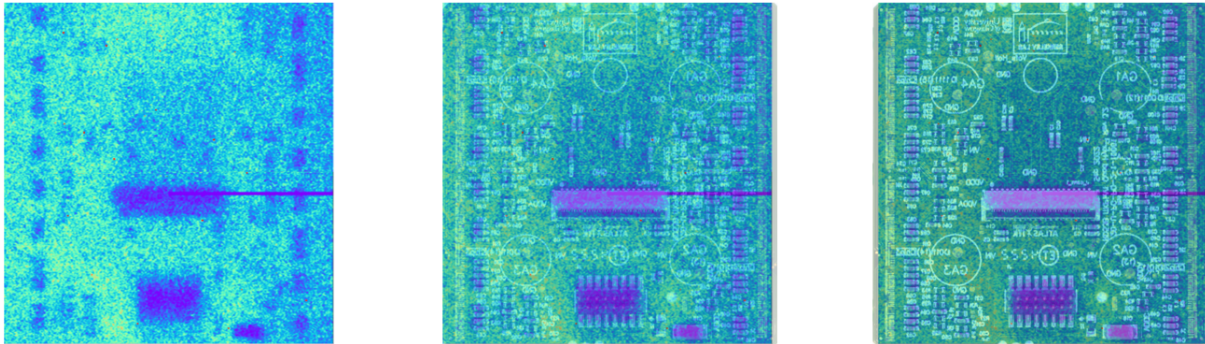
Figure 9.2: A source Scan performed on Q11 in a warm environment. For comparison, the flex is overlayed to the source Scan hit map with 100%, 75% and 60% transparency (from left to right).

9.2 Source Scan

The ^{90}Sr source emits β^- particles with a maximal energy of 546 keV. According to the Bethe-Bloch Formular 3.1, the energy loss per unit length for such energies is large resulting in a weak penetration power. The particles are absorbed in the SMD components on the flex, thus the SMD components on the flex are visible in source scan hit maps. The foam box of the cold setup further lowers the number of hits that were observed in a source scan in the cold setup. This will not affect the real service in HL-ATLAS, because as the pixel detector is right next to the beampipe the particles to detect will have energies in the magnitude of up to 100 GeV, which leads according to Bethe-Bloch (Equation 3.1) to a minimum ionising particle (MIP) like behaviour. So the real particles will have no problem going through any SMD components, nor any cables and will still have enough energy to pass the multiple layers of pixel detectors. Figure 9.2 compares the source scan hit map with the flex. That explains why even in a 5 hours-long source scan the pixels under the SMD components have barely more than 4 hits. It also explains the smaller peak of the source scan hit numbers of around 15 hits in the histogram in Figure 8.7. The selftrigger source scan, which is a new feature in RD53B, makes source scans roughly 60 times more efficient.

10 Summary and Outlook

The tests performed on the modules that are ITkPixV1.1 modules follow the instructions of the electrical specification and QC procedure for ITkPixV1.1 [49]. The procedure will be the same for production (ITkPixV2) and the modules will have to meet the same electrical QC except for the numerical values that might be adapted considering the results of preproduction.

The three modules that were investigated in this thesis show several problems in certain tests, especially the cold tests cause failing chips. For this reason, none of these modules will make it into the loaded local support preproduction nor the demonstrator for the ITk Pixel Detector, which are loaded with good preproduction modules. For the real cooling of the ITk modules, it is planned to stack the quad modules to local supports made out of carbon fibre. Part of these local supports are long and small cooling pipes, in which CO_2 gas flows for cooling. The temperature of the cooling gas is $-20\,°C$. To certify the module's operation in all possible circumstances, the tests are performed in warm and in cold environments.

To a certain degree, the problems that occurred were predicted from the results of the IV-curves and from VI. For production only BM and flexes that meet all criteria are assembled, securing a high production standard.

With the positive experience made within the scope of this thesis, the selftrigger method will continue to be used for source scan in production in order to handle the 1800 test cycles that have to be fulfilled. Also, it is worth trying to decrease the distance between the radioactive source and the module, by lifting the setup with the perspective to expedite the source scan, without limiting the cone of irradiation to a degree where it does not cover the module.

Outlook Unfortunately, because of logistical circumstances, the delamination test of the modules did not make it into this thesis. In thermal cycling, the persistency of the module under thermal alteration is probed. In the upcoming weeks, thermo cycles in a climate chamber are performed. This test exposes the modules to thermal stress to test the glue and bump bond quality with the perspective of verifying the long-term operation

in HL-Lʜᴄ including warm up during shutdowns.

The Aᴛʟᴀs Germany cluster will produce 1800 modules in total over the upcoming two years. The II. Institute of Physics in Göttingen builds 600 of these modules. Each module has to undergo an electrical test 3 times resulting in 1800 electrical cycles in the next two years. This demonstrates how urgent it is to fully automate the testing procedure. To be well prepared for the huge amount of electrical test cycles that are part of the ITkPix production which kicks-off in spring 2024, the setup in the source box will be upgraded as part of an internship.

Moreover, more preproduction modules are on the way to the II. Institute of Physics. These modules will be tested, building more routine and consolidating the test procedure Even though, the preproduction modules show some problems, especially in cold tests, the production phase is faced with curiosity. This thesis made a meaningful impact towards the profound understanding of the modules and the tests performed.

Bibliography

[1] R. L. Workman, et al. (Particle Data Group), *Review of Particle Physics*, PTEP **2022**, 083C01 (2022)

[2] S. L. Glashow, *Partial Symmetries of Weak Interactions*, Nucl. Phys. **22**, 579 (1961)

[3] S. Weinberg, *A Model of Leptons*, Phys. Rev. Lett. **19**, 1264 (1967)

[4] A. Salam, *Weak and Electromagnetic Interactions*, Almqvist & Wiksell, Stockholm, nobel symposium 8 edition (1968)

[5] S. L. Glashow, J. Iliopoulos, L. Maiani, *Weak Interactions with Lepton-Hadron Symmetry*, Phys. Rev. D **2**, 1285 (1970)

[6] H. Georgi, S. L. Glashow, *Unified Weak and Electromagnetic Interactions without Neutral Currents*, Phys. Rev. Lett. **28**, 1494 (1972)

[7] H. D. Politzer, *Reliable Perturbative Results for Strong Interactions*, Phys. Rev. Lett. **30**, 1346 (1973)

[8] H. D. Politzer, *Asymptotic Freedom: An Approach to Strong Interactions*, Phys. Rept. **14**, 129 (1974)

[9] D. J. Gross, F. Wilczek, *Asymptotically Free Gauge Theories*, Phys. Rev. D **8**, 3633 (1973)

[10] S. Weinberg, *The Making of the Standard Model*, Eur. Phys. J. C **34**, 5 (2004)

[11] G. 'tHooft, *Renormalization of massless Yang-Mills fields*, Nuclear Physics B **33(1)**, 173 (1971)

[12] G. 't Hooft, *Renormalizable Lagrangians For Massive Yang-Mills Fields*, Nucl. Phys. B **35**, 167 (1971)

[13] G. 't Hooft, M. Veltmann, *Regularization And Renormalization Of Gauge Fields*, Nucl. Phys. B **44**, 189 (1972)

Bibliography

[14] G. 't Hooft, M. Veltmann, *Combinatorics of gauge fields*, Nucl. Phys. B **50**, 318 (1972)

[15] H. Fritzsch, M. Gell-Mann, H. Leutwyler, *Advantages of the color octet gluon picture*, Phys. Lett. B **47(4)**, 365 (1973)

[16] M. Gell-Mann, *A Schematic Model of Baryons and Mesons*, Phys. Lett. **8**, 214 (1964)

[17] P. W. Higgs, *Broken Symmetries, Massless Particles and Gauge Fields*, Phys. Lett. **12**, 132 (1964)

[18] F. Englert, R. Brout, *Broken Symmetry and the Mass of Gauge Vector Mesons*, Phys. Rev. Lett. **13**, 321 (1964)

[19] P. W. Higgs, *Broken Symmetries and the Masses of Gauge Bosons*, Phys. Rev. Lett. **13**, 508 (1964)

[20] G. S. Guralnik, C. R. Hagen, T. W. B. Kibble, *Global Conservation Laws and Massless Particles*, Phys. Rev. Lett. **13**, 585 (1964)

[21] P. W. Higgs, *Spontaneous Symmetry Breakdown without Massless Bosons*, Phys. Rev. **145**, 1156 (1966)

[22] T. W. B. Kibble, *Symmetry Breaking in Non-Abelian Gauge Theories*, Phys. Rev. **155**, 1554 (1967)

[23] S. Tomonaga, *On a Relativistically Invariant Formulation of the Quantum Theory of Wave Fields**, Prog. Theor. Phys. **1(2)**, 27 (1946)

[24] J. Schwinger, *On Quantum-Electrodynamics and the Magnetic Moment of the Electron*, Phys. Rev. **73**, 416 (1948)

[25] J. Schwinger, *Quantum Electrodynamics. I. A Covariant Formulation*, Phys. Rev. **74**, 1439 (1948)

[26] R. P. Feynman, *Space-Time Approach to Quantum Electrodynamics*, Phys. Rev. **76**, 769 (1949)

[27] R. P. Feynman, *The Theory of Positrons*, Phys. Rev. **76**, 749 (1949)

[28] R. P. Feynman, *Mathematical Formulation of the Quantum Theory of Electromagnetic Interaction*, Phys. Rev. **80**, 440 (1950)

[29] F. J. Dyson, *The Radiation Theories of Tomonaga, Schwinger, and Feynman*, Phys. Rev. **75**, 486 (1949)

[30] F. J. Dyson, *The S Matrix in Quantum Electrodynamics*, Phys. Rev. **75**, 1736 (1949)

[31] H. Bethe, *Zur Theorie des Durchgangs schneller Korpuskularstrahlen durch Materie*, Ann. Phys. **397(3)**, 325 (1930)

[32] F. Bloch, *Zur Bremsung rasch bewegter Teilchen beim Durchgang durch Materie*, Ann. Phys. **408(3)**, 285 (1933)

[33] H. Kolanoski, N. Wermes, *Particle Detectors*, Oxford University Press (2020)

[34] E. Young, *Ultrafast acoustic strain generation and effects in semiconductor nanostructures*, Ph.D. thesis (2014)

[35] R. Nelms, R. Johnson, *200°C operation of a 500-W DC-DC converter utilizing power MOSFETs*, Industry Applications, IEEE Transactions on **33**, 1267 (1997)

[36] W. Shockley, *Currents to Conductors Induced by a Moving Point Charge*, J. Appl. Phys. **9(10)**, 635 (2004)

[37] S. Ramo, *Currents Induced by Electron Motion*, Proceedings of the IRE **27(9)**, 584 (1939)

[38] J. T. Boyd, *LHC Run-2 and Future Prospects* (2020), `2001.04370`

[39] The ATLAS Collaboration, *Observation of a new particle in the search for the Standard Model Higgs boson with the ATLAS detector at the LHC*, Phys. Lett. B **716**, 1 (2012)

[40] S. Chatrchyan, et al. (CMS), *Observation of a New Boson at a Mass of 125 GeV with the CMS Experiment at the LHC*, Phys. Lett. B **716**, 30 (2012)

[41] The ATLAS collaboration, *The ATLAS Experiment at the CERN Large Hadron Collider*, JINST **3**, S08003 (2008)

[42] N. Belyaev, et al., *Development of Transition Radiation Detectors for hadron identification at TeV energy scale*, J. Phys. Conf. Ser. **1390(1)**, 012126 (2019)

[43] D. Varouchas, *Flex metrology and visual inspection*, ATLAS internal note (2023)

[44] J. E. Metcalfe, *Bare Module IV*, ATLAS internal note (2023)

Bibliography

[45] D. Varouchas, *Assembly of real modules*, ATLAS internal note (2023)

[46] M. Janda, *Pixel bare Module, Sensor and FE chip Engineering DWG*, ATLAS internal note (2024)

[47] L. Cunningham, *Pixel Quad Module Assembly DWG*, ATLAS internal note (2023)

[48] Korea Atomic Energy Research Institute. Nuclear Data Evaluation Lab., *Nuclide Table* (2000)

[49] R. Bates, *Technical Specification for ITk Pixel Modules*, ATLAS internal note (2019)

Acknowledgement

Erklärung nach §13(9) der Prüfungsordnung für den Bachelor-Studiengang Physik und den Master-Studiengang Physik an der Universität Göttingen: Hiermit erkläre ich, dass ich diese Abschlussarbeit selbständig verfasst habe, keine anderen als die angegebenen Quellen und Hilfsmittel benutzt habe und alle Stellen, die wörtlich oder sinngemäß aus veröffentlichten Schriften entnommen wurden, als solche kenntlich gemacht habe.

Darüberhinaus erkläre ich, dass diese Abschlussarbeit nicht, auch nicht auszugsweise, im Rahmen einer nichtbestandenen Prüfung an dieser oder einer anderen Hochschule eingereicht wurde.

Göttingen, den 5. April 2024

(Niklas Grün)